International Immunology, Vol. 20, No. 3, pp. 317–326
doi:10.1093/intimm/dxm152

Tissue-specific expression of B-cell translocation gene 2 (*BTG2*) and its function in T-cell immune responses in a transgenic mouse model

Rafik Terra[1], Hongyu Luo[1], Xiaoying Qiao[1] and **Jiangping Wu[1,2]**

[1]The Laboratory of Immunology and [2]Nephrology Service, Centre hospitalier de l'Université de Montréal, Notre-Dame Hospital, Pavilion DeSève, 1560 Sherbrooke Street East, Montreal, Quebec H2L 4M1, Canada

Keywords: BTG2, circadian rhythm, *in situ* hybridization, T cells, transgenic mouse

Abstract

B-cell translocation gene 2 (*BTG2*) belongs to the anti-proliferative gene family. According to previous *in vitro* studies, *BTG2* overexpression leads to delayed cell cycling. We investigated *BTG2* expression during mouse ontogeny and its immune and circadian functions in this study. *In situ* hybridization showed that *BTG2* was expressed at high levels in the central nervous system, liver, stomach, thymus, spleen, skin, adrenal gland, pituitary gland and salivary glands during embryonic days (E10–E17), postnatal days (P1 and P10) and adult stages. Expression was observed in organs and tissues from adult mice with and without a robust proliferation program. Thus, the gene might have important functions that are both related and unrelated to proliferation. *BTG2* expression was induced after *in vitro* T-cell receptor stimulation in T cells using anti-CD3 antibodies. However, transgenic (Tg) mice with actin promoter-driven expression of *BTG2* showed normal *in vitro* and *in vivo* T-cell responses, such as thymus development, T-cell activation marker expression, T-cell proliferation and migration, as well as *in vivo* delayed-type hypersensitivity reactions. Although BTG2 was expressed in the suprachiasmatic nucleus and pineal gland in the brain, *BTG2* Tg mice had no abnormal circadian behavior. Our data on *BTG2* expression during ontogeny provide useful clues for the further investigation of BTG2 function. Additional studies are warranted to examine its role in immune and other systems.

Introduction

B-cell translocation gene 2 (*BTG2*) belongs to the anti-proliferative gene family, which consists of 19 members. *BTG2* contains a BTG-A box and a BTG-B box in its protein sequence (1), which are highly conserved among species. According to immunohistochemistry, *BTG2* is expressed in various organs and tissues, with high levels detected in the lung, kidney, intestine, pancreas and prostate (2). *BTG2* is located in the cytoplasm with a short half-life of ~15 min (3). Its expression is induced by growth factors (4) or DNA-damaging processes (5). *BTG2* seems to function as an adaptor, interacting with diverse molecules such as protein arginine methyltransferase PRMT1, homeobox protein Hoxb9, carbonylate repressor-associated factor Caf1, cyclin B1-associated kinase Cdc2, PKC-α binding protein PICK1, an ER-α coactivator CCR4 and peptidyl prolyl cis/trans isomerase Pin-1. Based mostly on *in vitro*-forced expression studies, *BTG2* has been shown to inhibit G1/S transition (1), induce G2/M arrest (1), augment apoptosis (1), enhance retinoic acid-induced differentiation of hematopoietic cells (6) and suppress thymocyte expansion (7). Reduced BTG2 expression is observed in some malignant tumors, suggesting its role as a tumor suppressor gene (8). However, these *in vitro* or correlative findings have not been confirmed in a *BTG2* null-mutant model *in vivo*. $BTG2^{-/-}$ mice are viable and fertile without a documented increase of malignancy (9). Their T- and B-cell development seems to be normal according to cell subpopulations in the thymus and spleen. The prominent phenotype of these mice is vertebrae malformation, underscoring the importance of this gene product in development and bone pattern formation.

In our ongoing study to investigate mechanisms of T-cell activation, we compared gene expression on resting versus activated T cells using DNA microarray. *BTG2* was among genes differentially expressed after TCR ligation of T cells. It was thus selected for further study on its expression during ontogeny, employing *in situ* hybridization (ISH). *BTG2*

Correspondence to: J. Wu; E-mail: jianping.wu@umontreal.ca

Received 15 September 2007, *accepted* 7 December 2007

Transmitting editor: A. Falus

Advance Access publication 14 January 2008

transgenic (Tg) mice were generated to explore the function of this gene in the immune system.

Methods

In situ *hybridization*

Full-length 2583-pb *BTG2* cDNA in pSPORT1 (clone H3059F09 from National Institute of Aging, Bethesda, MD, USA) was employed as a template for sense and anti-sense riboprobe synthesis, using SP6 and T7 RNA polymerase for both ^{35}S-UTP and ^{35}S-CTP incorporation (10).

Tissues were frozen in -35°C isopentane and kept at -80°C until sectioned. ISH was performed on 10-μm thick cryostat-cut slices, as outlined previously (10). Anatomic ISH was conducted with X-ray films.

Northern blot analysis

A partial *BTG2* cDNA fragment (clone H3059F09 from the National Institute of Aging, USA; mouse 15K cDNA clone sets; positions 1–2145 bp, according to the sequence of NM007570 in GeneBank) was labeled with a digoxin (Dig)-labeling kit from Roche Applied Sciences (Laval, Quebec, Canada). Total RNA was extracted from cultured cells with Trizol (Invitrogen, Burlington, Ontario, Canada). RNA (20 μg per lane) was resolved in 0.9% formaldehyde agarose gel and transferred to N-Hybond nylon membranes (Amersham Biosciences, Baie d'Urfe, Quebec, Canada). The membranes were hybridized with Dig-labeled probes, and the signals were revealed by a Dig detection kit (Roche Applied Sciences). Band intensities of 18S and 28S ribosomal RNA were indicators of even RNA loading.

Generation of BTG2 Tg mice

The 2145-bp mouse full-length *BTG2* cDNA was excised from pSPORT1 with SmaI/XbaI, and cloned into the BamHI (blunted)/XbaIs sites in vector pAC, between the human β-*actin* promoter and β-*actin* polyA signals. The resulting construct was named pAC-BTG2. The 7.4-kb ClaI/ClaI fragment containing the β-*actin* promoter, *BTG2* cDNA and β-actin polyA signal was excised and injected into fertilized C3H × C57BL/6 eggs. Genotyping of the Tg mice was first performed by Southern blot analysis. Tail DNA of the founders (10 μg per each) was digested with PstI and resolved by 1% agarose gel electrophoresis. The DNA was transferred onto N$^+$ Hybond nylon membranes after denaturation. A 4.2-kb band specific to the transgene was detected by the same Dig-labeled *BTG2* probe as was employed for northern blot analysis. Subsequent genotyping was undertaken by PCR. The 5′ and 3′ primers were AGGTGGCTTCGTCTCTCTTGCTTT and GAATGCAATTGTTGTTGGTAACTTG, respectively, for detection of a 550-bp band. The following PCR conditions were employed: 94°C × 5 min, 1 cycle; 94°C × 1 min, 55°C × 1 min, 72°C × 1 min, 30 cycles; 72°C × 5 min, 1 cycle.

Real-time reverse transcription–PCR

BTG2 mRNA in Tg and wild type (WT) cells was measured by real-time reverse transcription (RT)–PCR; the 5′ and 3′ primers were TGAGCGAGCAGAGACTCAAGGTTT and ACAGCGATAGCCAGAACCTTTGGA, respectively. A 112-bp product was detected with the following amplification program: 95°C × 15 min, 1 cycle; 94°C × 15 s, 55°C × 30 s, 72°C × 30 s, 40 cycles.

β-*actin* mRNA levels were measured as internal controls; the 5′ and 3′ primers were TGGTACCACAGGCATTGTGAT and TGATGTCACGCACGATTTCCCT, respectively, with the same amplification program as for *BTG2* mRNA.

Real-time PCR was performed in triplicate, and the signal ratios of *BTG2*/β-actin represented the normalized expression levels of *BTG2*.

Immunofluorescence

The cytofix/cytoperm kit (Pharmingen, San Diego, C, USA) was used for intracellular BTG2 staining. WT and Tg thymocytes and splenocytes were fixed and permeabilized with 250 μl Cytofix/Cytoperm solution for 20 min at 4°C. Cells were washed twice with 1 ml of Perm/Wash buffer and stained for 30 min in 100 μl Perm/Wash buffer with anti-BTG2 polyclonal antibody (Cedarlane laboratories, Hornby, ON, Canada). After two washes, cells were stained with the secondary antibody (FITC-anti-rabbit Ig F(ab′)2; Chemicon, Australia). Cells were then centrifuged on glass slides using a Cytospin (Shandon, Pittsburg, PA, USA). The cells were visualized under a fluorescent microscope.

Flow cytometry

The expression of CD3, CD4, CD8, CD19, CD25, CD44, CD69, Thy1.2 and B220 in thymocytes, splenocytes and lymph node (LN) cells was analyzed by flow cytometry as described in our previous publication (11). Different stages of double-negative (DN) subpopulations of adult thymocytes were analyzed by CD25 and CD44 staining on lineage-negative cells (12), which were gated with a mAb cocktail against CD3ε, CD11b, CD45R, B220, Ly6C, Ly6G, GR-1 and TER-119. Annexin V staining was conducted according to a procedure described earlier (11). All antibodies as well as annexin V–FITC were purchased from BD Pharmingen (San Diego, CA, USA), Cedarlane Laboratories (Hornby, Ontario, Canada) and Beckman Coulter (Mississauga, Ontario, Canada). Cells were analyzed on a Coulter flow cytometer with Expo32 software.

T- and B-cell proliferation

Thymocytes and spleen T and B cells were purified, cultured and stimulated according to established methods (11). Cell proliferation was measured by ^{3}H-thymidine uptake.

Delayed-type hypersensitivity assay

Mice were first primed by painting their shaved abdominal skin with FITC. On day 6, ear thickness was measured, and the ears were then challenged by FITC painting. Ear thickness was remeasured after 24 h on day 7, and any increases were registered. This method has been described elsewhere (11).

In vitro *LN cell migration assay*

In vitro migration assays were performed in Transwell chambers (6.5 mm in diameter, 5 μm pore size; Costar Corp.,

Cambridge, MA, USA), as detailed in our previous publication (13). The lower chamber contained 600 μl serum-free medium in the presence of stromal cell derived factor (SDF)-1α (80 ng ml^{-1}) from R & D Systems (Minneapolis, MN, USA). The upper chamber held 100 μl serum-free medium containing 0.3×10^6 T cells. The Transwell ensemble was then incubated at 37°C for 2 h, and T cells migrating into the lower chamber were counted by flow cytometry. All the samples were in duplicate.

Results

BTG2 expression during ontogeny

We employed ISH to map the *BTG2* expression pattern during ontogeny, starting from embryonic day 10 (E10) and in adult organs, using an anti-sense probe derived from *BTG2* cDNA.

BTG2 was expressed in the whole primordial nervous system at mid-gestation on E10 and E12 (Fig. 1A and B); its signals were very high in the mesencephalon, neural tube, spinal cord, myencephalon, primordial cerebellum, cranial flexure and optic chiasma. During the perinatal period from E17 to postnatal day 1 (P1), and the early postnatal stage at P10, *BTG2* expression was reduced in the nervous system in general, but high signals were detected in a few brain regions, such as the ventricular zone, olfactory turbinates, olfactory lobe and retina (Fig. 1D–F). Biphasic *BTG2* expression in the liver was noted. The first peak of expression was evident in the hepatic primordium on E12 and E15 (Fig. 1C), followed by a decline from E17 to P1 (Fig. 1D and E); the second expression peak was seen on P10 (Fig. 1F). BTG2 expression in the thymus and pulmonary tissue was induced at late gestation on E17 and remained high on P10 (Fig. 1D and F), at which time, expression in the spleen was also obvious (Fig. 1F). The skin and stomach wall started to show high *BTG2* expression on P10.

BTG2 mRNA in adult tissues

In the adult central nervous system (Fig. 2A–C), significantly concentrated *BTG2* mRNA was present in a few specialized structures, such as the ventricular zone, which is important in maintaining brain stem-cell population; the suprachiasmatic nucleus and pineal gland, both of which are involved in circadian rhythm regulation; the dentate gyrus, which is part of the hippocampal formation; the substantia nigra, which regulates involuntary motor activity; the olfactory lobe (Fig. 2C) and the spinal cord (Fig. 2D). In the endocrine system, both the intermediate and anterior lobes but not the posterior lobe of the pituitary gland were highly labeled (Fig. 2E); the signals were very high in both the cortex and medulla of the adrenal gland (Fig. 2F). Elevated *BTG2* mRNA levels were also found in the glandular and non-glandular regions of the stomach (Fig. 2M), submaxillary gland and sublingual gland (Fig. 2N). Intermediate levels of the *BTG2*

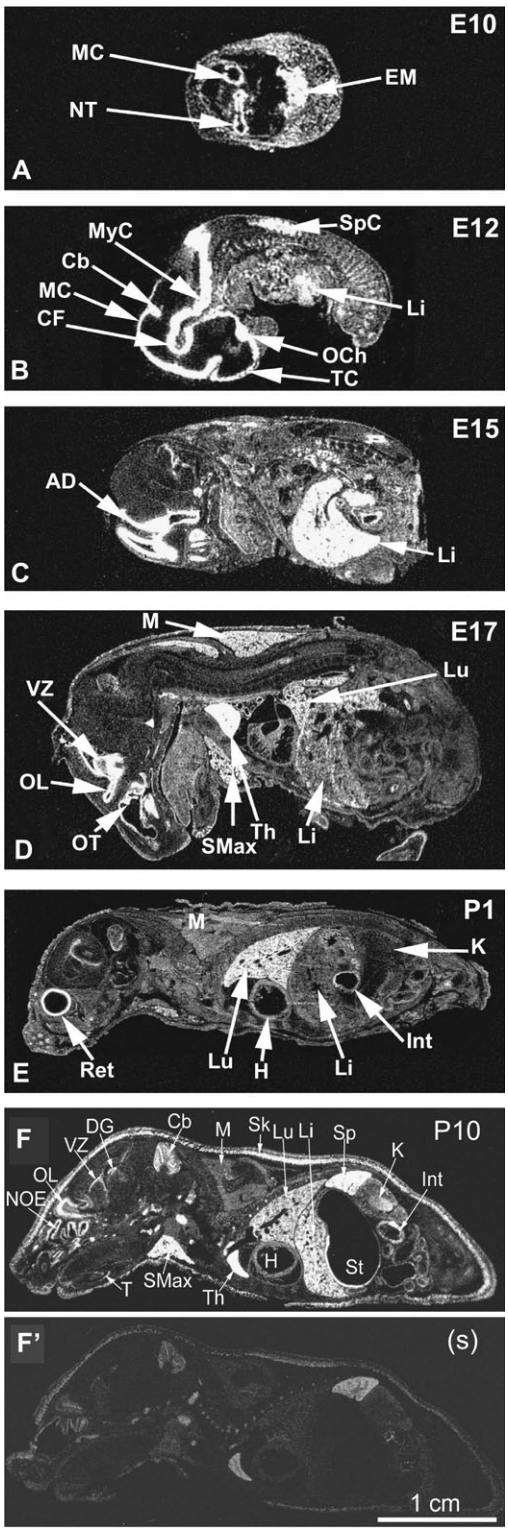

Fig. 1. *BTG2* expression during ontogeny according to ISH. X-ray autoradiography (dark field) of BTG2 ISH in mice from E10 to P10 is shown (A–F). Hybridization with the sense (S) probe is presented as control (F'). MC, mesencephalon; NT, neural tube; EM, embryonic membranes; MyC, myencephalon; Cb, cerebellum promordium; CF, cranial flexure; SpC, spinal cord; Li, liver, hepatic primordium; Och, optic chiasma; TC, telencephalon; AD, anterior part of the diencephalon; M, striated muscles; Lu, lung; VZ, ventricular zone; OL, primordial olfactory lobe; OT, olfactory turbinates; Th, thymus; Smax, submaxillary gland; Ret, retina; H, heart; Int, intestine; K, kidney; NOE, neuroolfactive epithelium; DG, dentate gyrus (part of the hippocampal formation in the brain); Sk, skin; Sp, spleen; St, stomach. Magnification scales and ages are indicated.

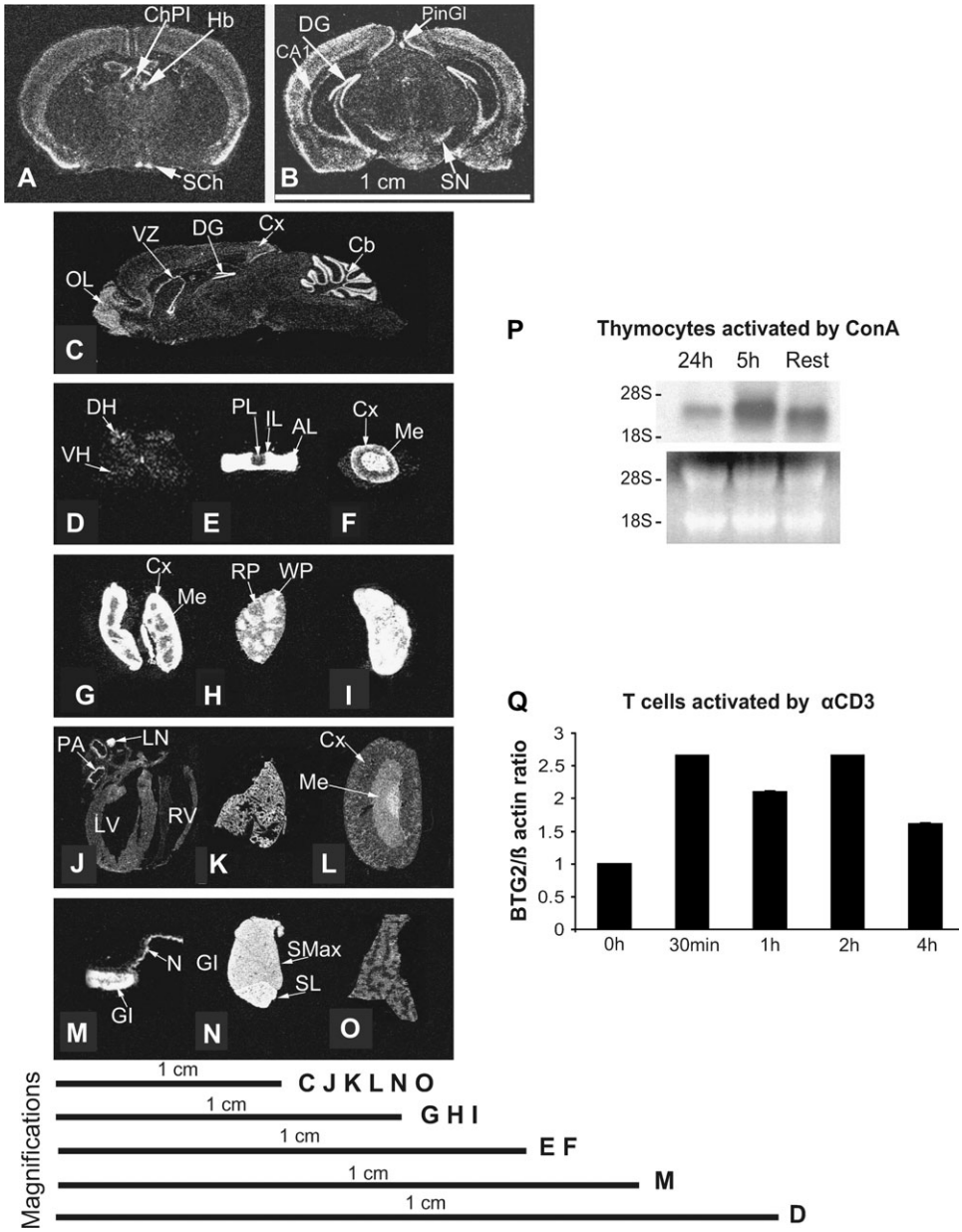

Fig. 2. *BTG2* expression in adult organs according to ISH. X-ray autoradiography (dark field) of ISH are shown. (A) and (B): sagittal brain sections. SC, suprachiasmatic nuclei; PinGl, pineal gland; Cal, CAl region in the hippocampus; ChPl, choroid plexus; DG, dentate gyrus; Hb, habenula; SN, substantia nigra. (C) Longitudinal brain section. VZ, ventricular zone; DG, dentate gyrus; Cx, cerebral cortex; Cb, cerebellum. (D) Spinal cord. DH, dorsal horn; VH, ventral horn. (E) Pituitary gland. IL, intermediate lobes; AL, anterior lobes; PL, posterior lobe. (F) Adrenal gland. Cx, cortex; Me, medulla. (G) Thymus. Cx, cortex; Me, medulla. (H) Spleen. WP, white pulp; RP, red pulp. (I) Lymph nodes. (J) Heart. LV, left ventricles; RV, right ventricles; PA, pulmonary arteries; LN, small lymph nodules. (K) Lung. (L) Kidney. Cx, cortex; Me, medulla. (M) Stomach. GI, glandular regions; N GI, non-glandular regions. (N) Salivary glands. Smax, submaxillary gland; SL, sublingual gland. (O) Liver. (P) Northern blot analysis of BTG2 expression in thymocytes. Thymocytes were activated by Con A (1.5 μg ml^{-1}), and spleen T cells were activated by soluble anti-CD3 (0.1 μg ml^{-1}). The duration of activation is indicated. Bands of 28S and 18S ribosomal RNA are presented to show RNA loading. (Q) Real-time RT–PCR analysis of BTG2 expression in T cells. Spleen T cells were activated by soluble anti-CD3 (0.1 μg ml^{-1}). The duration of activation is indicated. Means ± SD of ratios of BTG2 versus β-actin signals are shown.

signal were detected in the kidney medulla, pulmonary artery (Fig. 2J), lung (Fig. 2K) and liver (Fig. 2O).

BTG2 mRNA expression in adult lymphoid organs and T cells

Adult lymphoid organs, such as the thymus cortex (Fig. 2G), spleen white pulp (Fig. 2H) and LN (Fig. 2I), contained high levels of *BTG2* mRNA.

BTG2 expression during *in vitro* T-cell activation was investigated by northern blot analysis for thymocytes and real-time RT–PCR for spleen T cells. We found that the constitutive *BTG2* expression in unstimulated thymocytes and spleen T cells was relatively low, compared with activated cells (Fig. 2P and 2Q). Thymocytes and spleen T cells were stimulated *in vitro* with Con A and anti-CD3 (clone

2C11), respectively. Thymocytes were harvested at 5 and 24 h and spleen T cells, at 0 h, 30 min, 1, 2 and 4 h. As shown in Fig. 2P, one discrete band representing *BTG2* mRNA above the 18S ribosome marker was detected in unstimulated cells; its intensity increased after 5 h followed by a decline at 24 h. In spleen T cells, *BTG2* mRNA levels rose drastically after 30 min, and the high levels were maintained for at least 2 h (Fig. 2Q).

Generation of BTG2 Tg mice

To investigate *BTG2* functions not necessarily restricted to the immune system, Tg mice expressing human β-actin promoter-driven *BTG2* were generated. The plasmid construct for Tg mice generation is illustrated in (Fig. 3A). Two Tg founders (lines 17352 and 17657) were established. Line 17657 was selected for further experimentation because of its higher transgene copy number. PCR was performed for routine genotyping of Tg mice; Tg but not WT tail DNA displayed a 550-bp band (Fig. 3B). Increased *BTG2* mRNA expression in resting Tg thymocytes, LN cells and splenocytes was confirmed by real-time RT-PCR (Fig. 3C). BTG2 protein expression levels in Tg thymocytes and splenocytes were increased compared with WT cells, according to immunofluorescence (Fig. 3D). *BTG2* Tg mice were fertile and manifested no gross anomalies upon visual inspection.

BTG2 Tg mice presented normal thymocyte, splenocyte and LN cell subpopulations

BTG2 expression was drastically induced in thymocytes and T cells after their activation. This implies that the constitutive *BTG2* levels in these cells are not sufficient for the cell activation program. The effect of *BTG2* overexpression was studied in these cells using Tg mice to assess whether the augmentation of its constitutive level would disturb the development and function of these cells. Thymus and spleen size and cellularity in *BTG2* Tg mice were similar to those in WT mice (Fig. 4A). Flow cytometry analysis demonstrated that B-cell percentage ($CD19^+B220^+$) in the spleen and LN of Tg and WT mice was comparable (Fig. 4B). No apparent difference was observed in the percentages of $CD4^+CD8^+$ double-positive (DP), $CD4^+$ single-positive (SP) and $CD8^+$ SP subpopulations in the Tg versus WT thymus (Fig. 4C). CD4- versus CD8-cell ratios in the spleen and LN of Tg mice were comparable to those in WT controls (Fig. 4C).

We wondered whether *BTG2* overexpression might interfere with early thymocyte development. Fast-proliferating DN thymocytes from Tg and WT thymi were further divided into DN1 ($CD44^+CD25^-Lin^-$), DN2 ($CD44^+CD25^+Lin^-$), DN3 ($CD44^-CD25^+Lin^-$) and DN4 ($CD44^-CD25^-Lin^-$) subpopulations by flow cytometry, and compared, but, no discernible difference was evident (Fig. 4D).

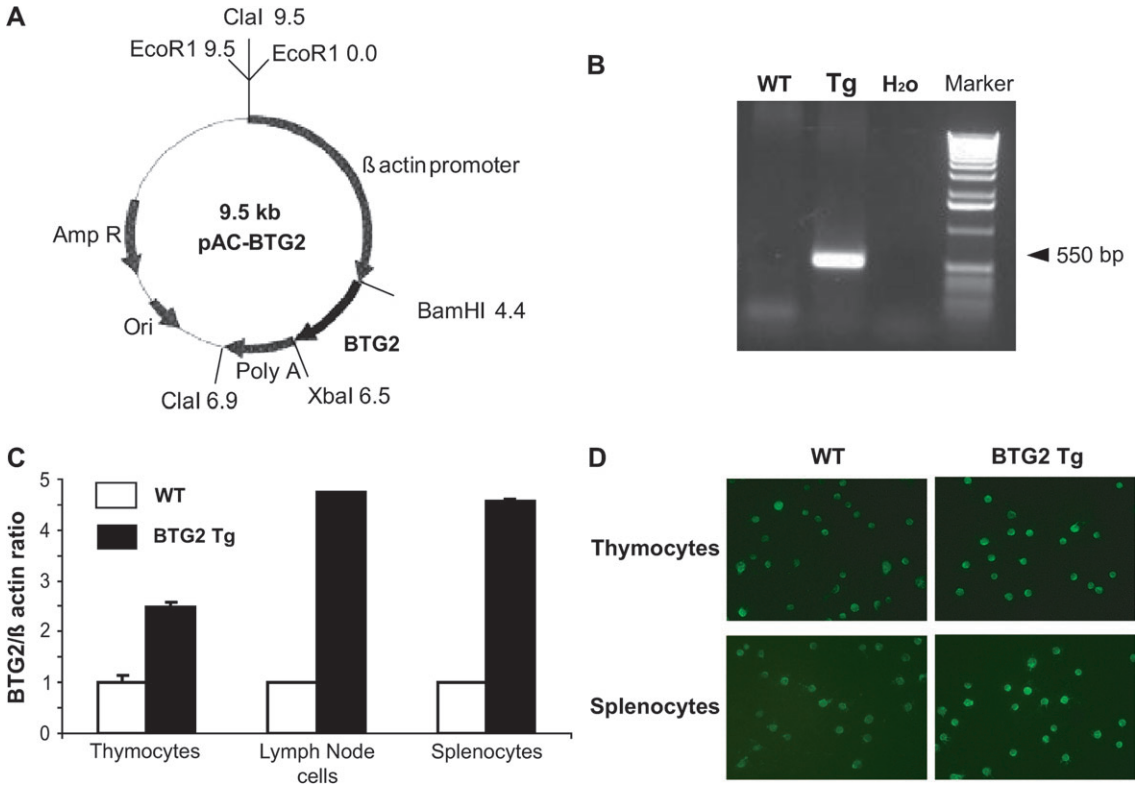

Fig. 3. Generation and characterization of *BTG2* Tg mice. (A) pAC-*BTG2* construct for Tg mice generation. The 7.4-kb ClaI/ClaI fragment was used for microinjection. (B) Genotyping of *BTG2* Tg founder tail DNA by PCR. The 428-bp band specific to the *BTG2* transgene is indicated by an arrow. (C) Real-time RT–PCR of *BTG2* mRNA from thymocytes, spleen and LN T cells. Means ± SD of ratios of *BTG2* versus β-*actin* signals from three pairs of Tg and WT mice are shown. (D) Immunofluorescent staining of BTG2 in WT versus Tg thymocytes and splenocytes. Permeabilized thymocytes and splenocytes were stained with rabbit anti-BTG2 antibody followed by the FITC–anti-rabbit antibody, and signals were registered by fluorescent microscopy.

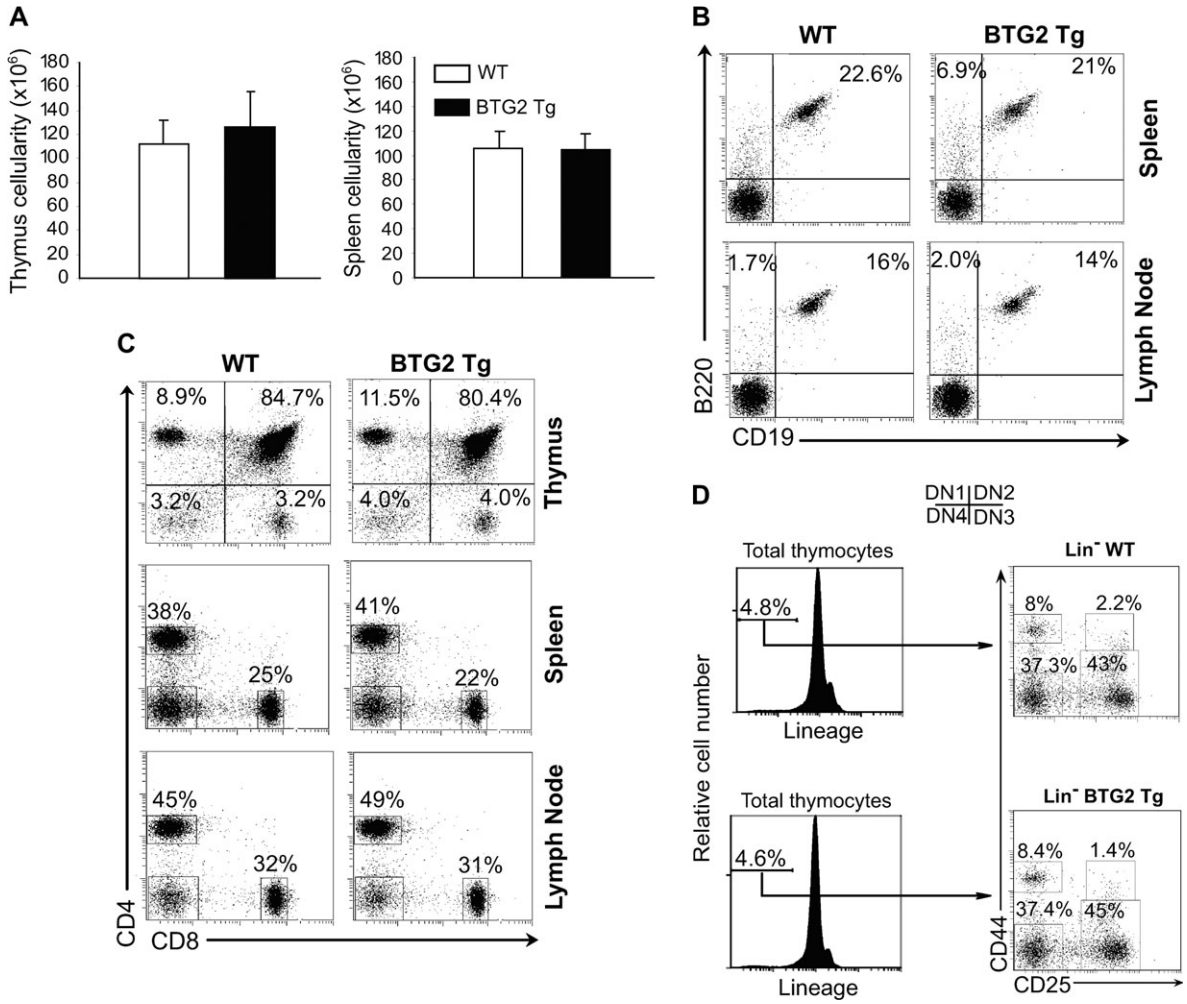

Fig. 4. Subpopulations of lymphocytes in *BTG2* Tg lymphoid organs. (A) Cellularity of the thymus and spleen. Tg mice and their WT littermates were compared for their thymus and spleen cellularity ($n = 5$). Means ± SD are shown. (B) DN thymocyte subpopulations. Thymocytes from Tg and WT mice were isolated and stained with lineage (Lin) markers (CD3ε, CD8β, TCRβ, CD11b, CD45R, B220, Ly6C, Ly6G, TER-119), CD25 and CD44 for three-color flow cytometry. Lin^- cells were gated and analyzed for their CD25 and CD44 expression. The percentages of DN1, DN2, DN3 and DN4 subpopulations are indicated. Representative data from three pairs of Tg and WT thymi are shown. (C) T-cell subpopulations in the thymus, spleen and LN. CD4 and CD8 T-cell populations in the Tg and WT thymus, spleen and LN were analyzed by two-color flow cytometry. The percentages are indicated. The experiments were repeated more than three times, and representative data are shown. (D) B-cell population in lymphoid organs. The B-cell population in the spleen and LN was analyzed by B220 and CD19 in two-color flow cytometry. The experiments were repeated three times, and representative data are shown.

In vitro *Tg lymphocyte function*

Compared with WT T cells, expression of the T-cell activation markers CD25, CD69 and CD44 was normal in Tg T cells stimulated by anti-CD3 or phorbol myristate acetate (PMA) plus ionomycin (Fig. 5A). Tg T-cell proliferation stimulated by anti-CD3, anti-CD3 plus anti-CD28 or PMA plus ionomycin was similar to that of WT T cells (Fig. 5B). Tg B cells also proliferated similarly to WT B cells under stimulation by IL-4 plus CD40L or IL-4 plus LPS (Fig. 5C). Tg LN cells chemotaxis toward SDF-1α showed no abnormality compared with WT cells, according to *in vitro* Transwell assays (Fig. 5D).

Apoptosis in Tg thymocytes and T cells

The reported *in vitro* apoptosis induced by forced *BTG2* expression led us to examine apoptosis in the T-cell compartment. Due to positive and negative selection, there is vigorous proliferation accompanied by massive apoptosis in the thymus. However, in freshly isolated thymocytes, there was no significant difference between all the stages examined, i.e. DN, DP and SP (Fig. 6A). We wondered whether the difference would only be revealed if external apoptotic signals were applied. Thus, Tg and WT thymocytes were treated with FasL and FasL plus cycloheximide, but no difference in their apoptosis was noted (Fig. 6B). The Tg and WT spleen T-cell apoptosis triggered by FasL was also similar (Fig. 6C). Thus, Tg *BTG2* overexpression did not seem to affect apoptosis of these cells.

In vivo *Tg T-cell function*

T-cell function *in vivo* was evaluated according to delayed-type hypersensitivity (DTH), a T-cell-dependent reaction. In the response measured 1 week after FITC skin priming, Tg

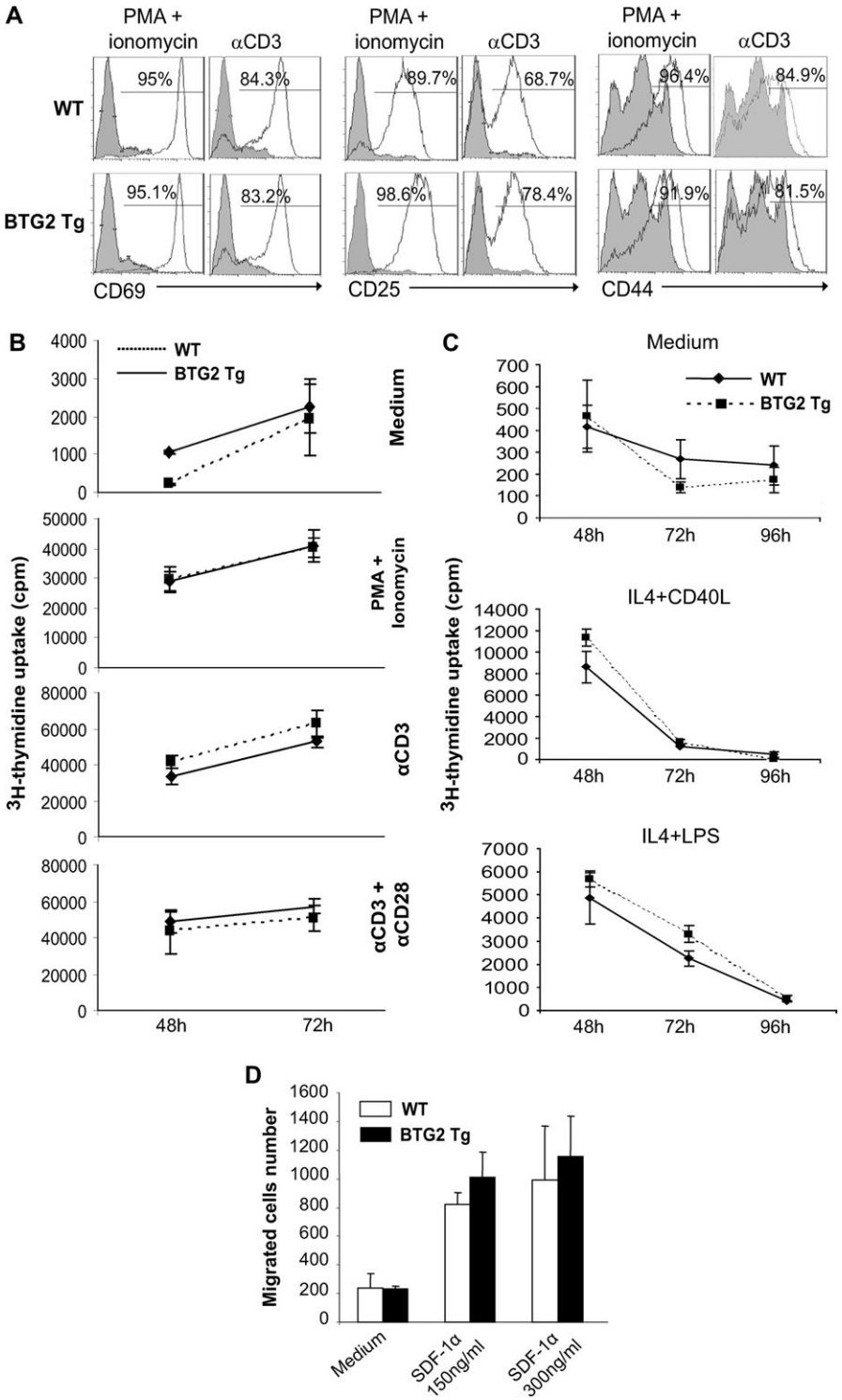

Fig. 5. Tg T- and B-cell functions *in vitro.* (A) C69, CD25 and CD44 expression on activated Tg T cells. Tg and WT T cells were stimulated overnight by solid phase anti-CD3 (4 μg ml^{-1}; concentration used for coating) or anti-CD3 plus anti-CD28 (0.57 and 2.86 μg ml^{-1}, respectively). CD69, CD25 and CD44 expression on Thy-1.2-gated T cells was measured by two-color flow cytometry. Shadowed areas represent cells cultured in medium. (B) Tg T-cell proliferation. Tg and WT spleen T cells were stimulated by soluble PMA (10 nM) plus ionomycin (0.1 μg ml^{-1}), solid phase anti-CD3 (4 μg ml^{-1}) or solid phase anti-CD3 (0.57 μg ml^{-1}) plus anti-CD28 (2.86 μg ml^{-1}) as indicated. The cells were pulsed with ^{3}H-thymidine 16 h before harvesting. ^{3}H-thymidine uptake of the cells was measured at 48 and 72 h. The samples were in triplicate, and means ± SD of cpm are shown. (C) Tg B-cell proliferation. Spleen non-T cells were stimulated with IL-4 (20 ng ml^{-1}) plus CD40L (0.1 μg ml^{-1}) or IL-4 (20 ng ml^{-1}) plus LPS (10 μg ml^{-1}). ^{3}H-thymidine uptake was measured in triplicate at 48, 72 and 96 h after the initiation of culture. Means ± SD of cpm are shown. (D) Tg LN cell migration toward SDF-1α. Means ± SD of the percentage of LN cell migration toward SDF-1α in the lower Transwell chamber measured by flow cytometry. The samples were in duplicate. The experiments in this figure were repeated three times, and representative data are shown.

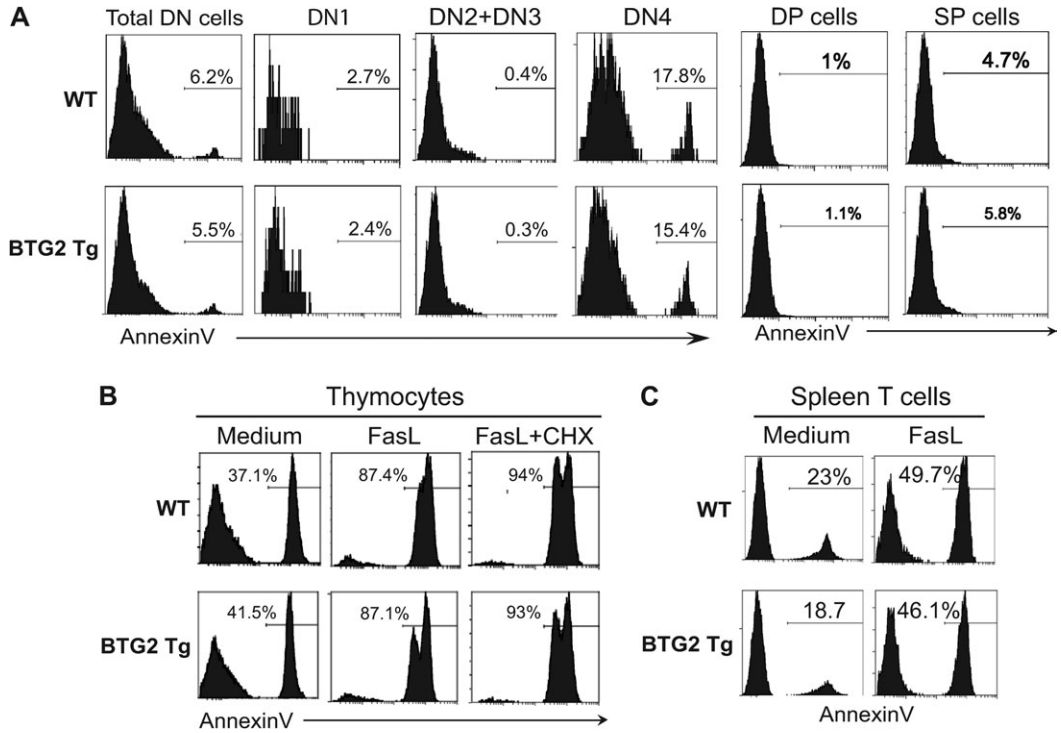

Fig. 6. Tg thymocytes and T-cell apoptosis. (A) Apoptosis of freshly isolated Tg thymocytes. Freshly isolated Tg and WT thymocytes were stained with annexin V and developmental markers (Lin, CD25, CD44, CD4 and CD8) and analyzed by three-color flow cytometry. The percentages of annexin V-positive cells are indicated. (B) Apoptosis of Tg thymocytes stimulated by FasL and cycloheximide (CHX). Tg and WT thymocytes were stimulated with FasL (0.2 μg ml^{-1}) or FasL plus CHX (0.5 μM) for 20 h. The cells were then stained with annexin V and analyzed by flow cytometry. (C) Apoptosis of Tg spleen T cells stimulated by FasL. Tg and WT spleen T cells were stimulated with FasL (0.2 μg ml^{-1}) for 20 h, and their apoptosis was analyzed by annexin V staining in flow cytometry. The experiments in this figure were repeated twice, and representative data are shown.

and WT mice exhibited similar percentages of ear thickness increment (Fig. 7).

BTG2 Tg mice displayed normal circadian rhythm

Our ISH analysis demonstrated that *BTG2* mRNA was expressed at high levels in the suprachiasmatic nucleus and pineal gland, both of which are involved in circadian rhythm regulation. The circadian activity of Tg mice was examined with the use of running wheels. The mice were kept under 12-h light and 12-h dark cycles. Tg and WT all followed precise activity rhythms, i.e. running the wheels only during the dark cycles, and no anomaly was observed (Fig. 8).

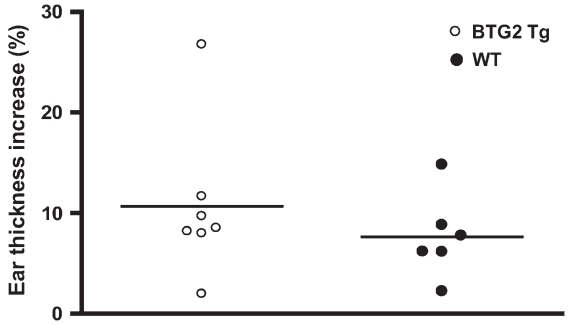

Fig. 7. Normal DTH in Tg mice. Tg mice and their WT littermates were tested for DTH. Ear thickness was measured three times, and mean values were registered. The percentage increase in ear thickness of each mouse was calculated as follows: % increase = (mean ear thickness 24 h after ear painting with FITC – mean ear thickness before ear painting)/mean ear thickness before ear painting. Horizontal bars represent the group means.

Discussion

Previous *in vitro* studies showed that *BTG2* overexpression hinders cell-cycle progress. Although *BTG2* null-mutant mice have been generated, there are no reports describing abnormal cell cycling in $BTG2^{-/-}$ cells. Additional studies are required to elucidate whether *BTG2* function is primarily in cell-cycle control. In this study, we took two approaches to this end. First, ISH was employed to map its expression during ontogeny and in adulthood. Subsequently, Tg mice with *actin* promoter-driven universal *BTG2* expression were generated to explore the function of this gene, with emphasis on the immune system and T-cell proliferation.

According to our ISH study, *BTG2* was expressed in several organs and tissues containing fast-proliferating cells, such as the thymus, skin and stomach. Northern blotting also indicates that its expression was augmented 5 h after thymocyte activation and 30 min after spleen T cells activation, which was in the beginning of G0 to G1 transition. Such findings suggest that this gene probably has functions other

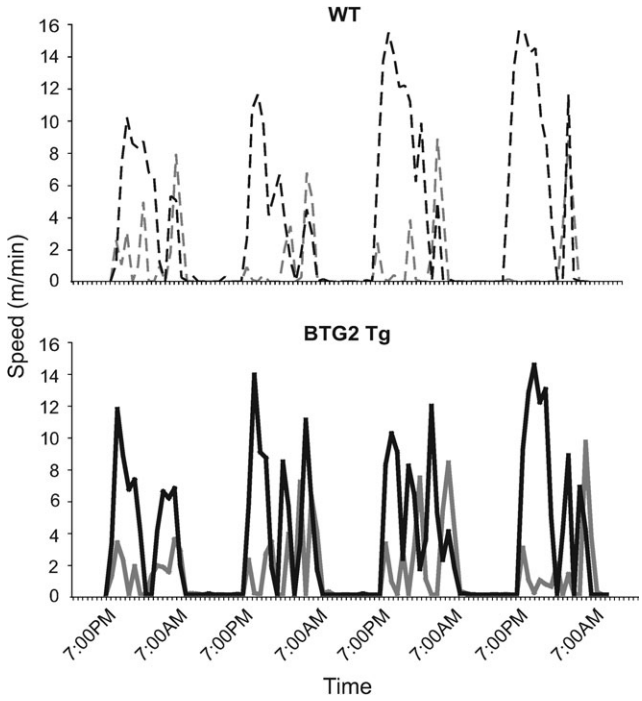

Fig. 8. Tg mice presented normal circadian activity. Tg and their WT littermates were housed in cages with running wheels with 12-h light/dark cycles. Their running activities in terms running speed (meter per minute) were recorded from day 2 to day 6. The results of two WT (black and gray solid lines) and two *BTG2* Tg (black and gray dotted lines) mice are shown.

than damping cell-cycle progress. This notion is further supported by the fact that many particular regions in the central nervous system, where regulation of proliferative activity is not required, also express high *BTG2* levels. Thus, BTG2 likely has function outsides the cell-cycling program.

BTG2 expression in the WT suprachiasmatic nucleus and pineal gland raised the possibility that this gene is involved in circadian regulation. However, Tg mice had normal circadian activity based on running wheel tests. They also adapted rapidly to forced 12-h delay of light/dark cycles, as did WT mice (data not shown). As *actin*-promoter-driven *BTG2* overexpression does not affect the circadian rhythm, it will be interesting to examine circadian activity in *BTG2*$^{-/-}$ mice.

In adulthood, relatively high-level *BTG2* transcription occurred in the adrenal cortex and medulla, pointing to its possible involvement in steroid and catecholamine synthesis and/or secretion.

BTG2 was expressed at high levels in the thymus, starting on E17, and its expression there remained high in adulthood. The spleen white pulp and LN also expressed *BTG2* levels higher than neighboring tissues. However, when examined quantitatively using northern blotting and real-time PCR, it was found that resting thymocytes and spleen T cells had basal *BTG2* expression, and such expression was rapidly augmented 3- to 4-fold after activation. This implies that the basal *BTG2* expression is not sufficient to cope with the requirement of activated T cells. This prompted us to investigate whether basal *BTG2* overexpression in thymocytes and resting T cells, using a Tg approach, would disturb their differentiation and function. Our Tg overexpression approach was also prompted by Konrad's observation that *BTG2/TIS21* overexpression using a retroviral expression system in thymocyte progenitors led to delayed progression of thymocytes at the DN2 and DN3 stages and at the DN to DP transition in fetal thymus organ culture and OP9-DL1 co-culture model (7). However, when the gene was overexpressed in Tg mice, according to all the tests we performed *in vitro* and *in vivo*, T cells seemed to show no anomaly in terms of their development, activation, proliferation, migration and *in vivo* DTH. There could be several explanations for such observations. Most likely, endogenous *BTG2* expression was more than sufficient for T-cell functions; therefore, the increased expression in Tg T cells minimally further influenced the function of this gene. It is also possible that the 2- to 5-fold rise in *BTG2* expression in Tg thymocytes and T cells was not sufficient to disturb T-cell biology. Indeed, Konrad and Zuniga-Pflucker (7) have observed delayed progression of thymocytes at the DN stages and at DN to DP transition after *BTG2* overexpression in thymocytes. The reason we did not observe such a delay is probably due to that the expression in our system was not sufficiently high, compared with Konrad's system (7). Lastly, we cannot rule out that there are undiscovered abnormal functions in immune as well as in other systems of Tg mice. In any case, such negative results are not findings that could be predicted a priori.

The human genome project revealed far fewer genes than expected. This leads to the speculation that not only the gene products but also their expression levels are important in modulating cell functions. The ISH reveals gene expression levels in constitutive status, but we really do not know what should be considered as high or low expression until all the stimulated status of cells are tested. Therefore, unbiased investigation using overexpression and knockdown/knockout should be conducted to elucidate functions of genes concerned. We cannot determine a priori which one of these approaches will reveal discernable phenotype, and both approaches are justified, as attempted here in this study using *BTG2* Tg overexpression.

Funding

Canadian Institutes of Health Research (CIHR, MOP57697 and MOP69089); the Kidney Foundation of Canada; the Heart and Stroke Foundation of Quebec; the Juvenile Diabetes Research Foundation, USA (1-2005-197); the J.-Louis Levesque Foundation to J.W. Group grants from Genome Canada/Quebec, the CIHR for New Emerging Teams in Transplantation, and Fonds de la recherche en santé du Québec (FRSQ) for Transfusional and Hemovigilance Medical Research to J.W.; CIHR (MOP79565) to H.L; National Scholarship to J.W.; Postdoctoral training grant from the FRSQ and CHIR/Rx&D-Wyeth Pharmaceuticals research fellowship program to R.T.

Acknowledgements

The authors thank Ovid Da Silva for his editorial assistance, Martin Marcinkiewicz for ISH analysis and the Core Facility of the New Emerging Team of Transplantation for DNA microarray analysis.

Abbreviations

BTG2	B-cell translocation gene 2
DN	double negative
DP	double positive
DTH	delayed-type hypersensitivity
E	embryonic day
ISH	*in situ* hybridization
Lin	lineage
LN	lymph node
P	postnatal day
PMA	phorbol myristate acetate
RT	reverse transcription
SDF	stromal cell derived factor
SP	single positive
Tg	transgenic
WT	wild type

References

1 Lim, I. K. 2006. TIS21 (/BTG2/PC3) as a link between ageing and cancer: cell cycle regulator and endogenous cell death molecule. *J. Cancer Res. Clin. Oncol.* 132:417.

2 Melamed, J., Kernizan, S. and Walden, P. D. 2002. Expression of B-cell translocation gene 2 protein in normal human tissues. *Tissue Cell* 34:28.

3 Varnum, B. C., Reddy, S. T., Koski, R. A. and Herschman, H. R. 1994. Synthesis, degradation, and subcellular localization of proteins encoded by the primary response genes TIS7/PC4 and TIS21/PC3. *J. Cell. Physiol.* 158:205.

4 Fletcher, B. S., Lim, R. W., Varnum, B. C., Kujubu, D. A., Koski, R. A. and Herschman, H. R. 1991. Structure and expression of TIS21, a primary response gene induced by growth factors and tumor promoters. *J. Biol. Chem.* 266:14511.

5 Rouault, J. P., Falette, N., Guehenneux, F. *et al.* 1996. Identification of BTG2, an antiproliferative p53-dependent component of the DNA damage cellular response pathway. *Nat. Genet.* 14: 482.

6 Passeri, D., Marcucci, A., Rizzo, G. *et al.* 2006. Btg2 enhances retinoic acid-induced differentiation by modulating histone H4 methylation and acetylation. *Mol. Cell. Biol.* 26:5023.

7 Konrad, M. A. and Zuniga-Pflucker, J. C. 2005. The BTG/TOB family protein TIS21 regulates stage-specific proliferation of developing thymocytes. *Eur. J. Immunol.* 35:3030.

8 Duriez, C., Falette, N., Audoynaud, C. *et al.* 2002. The human BTG2/TIS21/PC3 gene: genomic structure, transcriptional regulation and evaluation as a candidate tumor suppressor gene. *Gene* 282:207.

9 Park, S., Lee, Y. J., Lee, H. J. *et al.* 2004. B-cell translocation gene 2 (Btg2) regulates vertebral patterning by modulating bone morphogenetic protein/smad signaling. *Mol. Cell. Biol.* 24:10256.

10 Marcinkiewicz, M. 2002. BetaAPP and furin mRNA concentrates in immature senile plaques in the brain of Alzheimer patients. *J. Neuropathol. Exp. Neurol.* 61:815.

11 Luo, H., Yu, G., Tremblay, J. and Wu, J. 2004. EphB6-null mutation results in compromised T cell function. *J. Clin. Invest.* 114: 1762.

12 Terra, R., Louis, I., Le Blanc, R., Ouellet, S., Zuniga-Pflucker, J. C. and Perreault, C. 2005. T-cell generation by lymph node resident progenitor cells. *Blood* 106:193.

13 Shi, G., Wu, Y., Zhang, J. and Wu, J. 2003. Death decoy receptor TR6/DcR3 inhibits T cell chemotaxis in vitro and in vivo. *J. Immunol.* 171:3407.